The DOI for this manuscript is doi: 10.1175/JCLI-D-15-0438.1

The final published version of this manuscript will replace the preliminary version at the above DOI once it is available.

If you would like to cite this EOR in a separate work, please use the following full citation:

Yang, C., S. Masina, A. Bellucci, and A. Storto, 2016: The rapid warming of the North Atlantic Ocean in the mid-1990s in an eddy permitting ocean reanalysis (1982-2013). J. Climate. doi:10.1175/JCLI-D-15-0438.1, in press.

The rapid warming of the North Atlantic Ocean in the mid-1990s in an eddy permitting ocean reanalysis (1982-2013)

Chunxue Yang[1], Simona Masina[1,2], Alessio Bellucci[1] and Andrea Storto[1]

[1]Centro Euro-Mediterraneo per i Cambiamenti Climatici, Bologna, Italy

[2]Istituto Nazionale di Geofisica e Vulcanologia, Bologna, Italy

Corresponding author address: Chunxue Yang, Via M. Franceschini, 31, Bologna, Italy, 40128

Email: chunxue.yang@cmcc.it

Abstract

The rapid warming in the mid-1990s in the North Atlantic Ocean is investigated by means of an eddy-permitting ocean reanalysis. Both the mean state and variability, including the mid-1990s warming event, are well captured by the reanalysis. An ocean heat budget applied to the subpolar region (SPG) (50°N-66°N, 60°W-10°W) shows that the 1995-1999 rapid warming is primarily dictated by changes in the heat transport convergence term while the surface heat fluxes appear to play a minor role. The mean negative temperature increment suggests a warm bias in the model and data assimilation corrects the mean state of the model, but it is not crucial to reconstruct the time variability of the upper ocean temperature. The decomposition of the heat transport across the southern edge of SPG into time-mean and time-varying components, shows that the SPG warming is mainly associated with both the anomalous advection of mean temperature and the mean advection of temperature anomalies across the 50°N zonal section. The relative contributions of the Atlantic Ocean Meridional Circulation (AMOC) and gyre circulation to the heat transport are also analyzed. It is shown that both the overturning and gyre components are relevant to the mid-1990s warming. In particular the fast adjustment of the barotropic circulation response to the NAO drives the anomalous transport of mean temperature at the subtropical/subpolar boundary, while the slowly evolving AMOC feeds the large-scale advection of thermal anomalies across 50°N. The persistently positive phase of the NAO during the years prior to the rapid warming, did likely favour the cross-gyre heat transfer and the following SPG warming.

1. Introduction

The North Atlantic ocean plays an important role in several aspects of the global climate. Changes in the North Atlantic state have well established impacts on European and North American climate [Sutton and Dong, 2012; Sutton and Hodson, 2005], the frequency of Atlantic hurricane [Smith et al., 2010], marine ecosystem [Hátún et al., 2009], Greenland ice sheet [Holland et al., 2008], and also tropical Pacific climate [McGregor et al., 2014].

The observational records of North Atlantic sea surface temperatures (SSTs) reveal significant variability at the multi-decadal scale [Kushnir, 1994; Sutton and Hodson, 2003; Dommenget and Latif 2000; Ting et al., 2009, Hurrell and Deser, 2009]. In the mid-1990s, an abrupt warming of the northern North Atlantic, accompanied by a weakening and shrinking of the Subpolar Gyre (SPG) was observed [Häkkinen and Rhines, 2004]. This rapid warming has been shown in observations [Bersch et al. 2007; Sarafanov et al., 2008], and further corroborated by several model studies [Marsh et al. 2008, Lohmann et al., 2009a; Lohmann et al., 2009b; Grist et al., 2010; Yeager et al., 2012; Robson et al., 2012a; Desbruyères et al., 2014; Barrier et al., 2015].

Different physical mechanisms have been proposed for this rapid warming. An important driver of the North Atlantic variability, significantly impacting its properties and circulations, is the North Atlantic Oscillation (NAO) [Visbeck et al., 2003]. The NAO displays a predominantly positive phase from the beginning of the 1970s until the mid of 1990s. Between winters 1994/1995 and 1995/1996, the NAO underwent a sudden change from a positive to a negative phase, and since then it has been largely neutral [Hurrel and Deser, 2009]. A positive phase of the NAO is typically associated with stronger than normal westerly winds that cool down the surface of the subpolar region by increasing the latent heat fluxes. By using numerical models, Eden and Willebrand [2001] and Bellucci and Richards [2006] show that changes in the wind stress associated with the NAO are responsible for changes in the ocean circulation over the subpolar region. Brauch and Gerdes [2005] also suggest that the detected change in the SPG is caused by the change of the NAO, especially the sudden drop of the NAO index between 1994/1995 and 1995/1996 winters. Herbaut and Houssais [2009] and Häkkinen et al. [2011] argue that changes in the eastern SPG are mainly driven by a local response to the wind stress associated to the mid-1990s shift of the NAO phase. By performing a set of sensitivity experiments with an ocean general circulation model forced with an atmospheric reanalysis, Lohmann et al. [2009b] suggests that the combination of the ocean state preconditioning determined by the strong positive NAO in the years preceding 1995, and the sudden switch to a negative phase during winter 1995/1996 were responsible for the weakening of the SPG. The weakening and shrinking of the SPG that comes with a northwest shift of the subpolar front and also a northward advection of warm subtropical water in the Subpolar Gyre [Hátún et al., 2005, Bersch et al., 2007; Sarafanov et al., 2008] results in a warmer state in the SPG region. By using the same ocean model and atmospheric forcing as Lohmann et al. [2009b], Robson et al. [2012a] show that due to the positive NAO between the 1970s to the beginning of the 1990s, the Atlantic Meridional Overturning Circulation (AMOC) has been strengthening as a response to the enhanced buoyancy losses. The strengthening of AMOC results in an increase of the meridional heat transport, which brings more heat from the subtropical Atlantic to the Subpolar Gyre region. Therefore, they suggest that positive NAO phase is the primary driver of the meridional heat transport that accounts for the observed rapid warming in the SPG region. The delayed ocean response to the positive NAO implies some degree of predictability associated with this rapid warming event. With a set of decadal prediction experiments performed with different prediction systems, Robson [2012b], Yeager et al. [2012] and Msadek et al. [2014] show, in a broadly consistent way, that the increasing heat transport associated with stronger AMOC due to the positive NAO is responsible for the warming in the SPG region.

In a recent study, Barrier et al. [2015] investigate the North Atlantic warming by splitting the SPG region into western and eastern sub-basins. The authors pose a boundary in correspondence of the Rekjanes/Mid-Atlantic Ridge to separate western and eastern sub-region based on the different hydrographic properties characterizing the water masses in the two basins [Thierry et al., 2008]. Their results show that in the western Subpolar Gyre, the warming is the ocean response to the heat losses in the western SPG area determined by the positive NAO phase, resulting in an intensified deep convection that induces a strengthening of the AMOC. This in turn determines an increased meridional heat transport leading to the warming of the western SPG. On the other hand, the eastern SPG warming appears to be due to the barotropic adjustment of the gyre circulation, following the abrupt change of NAO from a positive to negative phase.

Previous studies have investigated the mid-1990s rapid warming event in the North Atlantic using observations, model simulations or decadal prediction experiments. To the authors' knowledge, there is no study tackling this issue based on an ocean reanalysis product. Ocean reanalyses are data sets that combine observations and numerical models through data assimilation methods, providing a more accurate and dynamically consistent estimate of the changing ocean state compared to either purely observational or model-only products. Analyzing the mid-1990s warming event in an ocean reanalysis will cover an important gap in the existing literature, allowing for a detailed understanding of the underlying processes, corroborated by the strong observational constraint embedded in the ocean reanalysis.

In this paper, we use an eddy-permitting ocean reanalysis to investigate the possible mechanisms of the rapid warming in the North Atlantic Ocean over the Subpolar Gyre region. The impact of data assimilation on the heat budget in a closed basin is also discussed. Section 2 describes the ocean reanalysis used for this study. In section 3, the warming phenomenon in the North Atlantic SPG region is described and analysed and a possible mechanism is proposed. Section 4 gives the summary and conclusions of this study.

2. Methods

For this study we used data from the global ocean reanalysis based on the Centro Euro-Mediterraneo sui Cambiamenti Climatici (CMCC) eddy-permitting Global Ocean Reanalysis System (C-GLORS) [Storto et al., 2015b], covering the 1982-2013 period and available at www.cmcc.it/c-glors and through the Copernicus Marine Service (marine.copernicus.eu). C-GLORS is based on NEMO 3.2.1 global ocean general circulation model [Madec et al., 1998] with an approximated ¼ degree horizontal resolution, ranging from about 10km at high latitude to 22km at mid-latitude and 27km at the Equator and 50 vertical levels with partial steps [Barnier et al., 2006]. The grid of the model is tri-polar, with two Poles on the Asian and North American continents and the third one at the South Pole. The vertical mixing parameterization is based on a turbulent kinetic energy (TKE) prognostic equation, whereas the Total Variation Diminishing (TVD) [Zalesak, 1979] algorithm is used as advection scheme. For the river runoff a monthly climatology from Dai and Trenberth

[2002], including 99 major rivers and coastal runoffs is used. A three-layers (two layers of sea ice and one layer of snow) dynamic-thermodynamic sea ice model, the Louvain-La-Neuve Ice Model, version 2 (LIM 2, Fichefet and Morales Maqueda, 1997) is coupled with the ocean component with a coupling frequency of 1.5 hours.

The atmospheric reanalysis from European Centre for Medium-Range Weather Forecast (ECMWF), ERA-Interim [Dee et al., 2011] is used as the surface forcing for C-GLORS. Surface wind (U and V at 10m) from ERA-Interim is used to calculate surface momentum fluxes using the CORE bulk formula [Large and Yeager, 2004]. Three hourly 2-meter air temperature and specific humidity, daily short-wave radiation, long-wave radiation, precipitation and snow from ERA-Interim are used for calculating heat and fresh water fluxes. The radiation fluxes from the ERA-Interim are corrected before used in C-GLORS due to the biases in the upwelling areas in the tropical oceans. The correction is based on Dussin and Barnier [2013]. Precipitation is also corrected by using a climatological correction coefficient derived from Remote Sensing Systems/Passive Microwave Water Cycle (REMSS/PMWC, see details in Storto et al. [2015b]).

The observations assimilated in C-GLORS include in-situ temperature and salinity profiles from ENSEMBLES EN3v2a (hereafter EN3) dataset [Ingleby and Huddleston, 2007] collected, distributed and quality checked by U.K. Met Office Hadley Center. EN3 includes observations from moorings, Argo floats, Expendable Bathy Thermographs (XBT), and Conductivity Temperature Depth (CTDs) devices. The XBT fall rate is corrected based on Wijffels et al. [2008]. Sea level anomalies are from the AVISO along-track delayed mode dataset that includes observations from ERS-1 and -2, Envisat, GFO, Jason-1 and -2, Topex/Poseidon and Cryosat-2. Sea surface temperature from the National Oceanic and Atmospheric Administration

(NOAA) high-resolution daily analyses [Reynolds et al., 2007] and sea ice concentration observations from the Defense Meteorological Satellite Program (DMSP) microwave radiances [Cavalieri et al., 1996] are also assimilated through a nudging scheme.

In-situ temperature and salinity profile data are assimilated by using a three-dimensional variational (3D-Var) assimilation scheme, as described in details in Storto et al. [2011] and Storto et al. [2014]. The analysis is performed every 7 days. The reanalysis system implements a three dimensional large-scale (time scales longer than 3 months and radial spatial scale longer than 2000km) bias correction on temperature and salinity to reduce spurious model biases and drifts. The bias is defined as the differences between model and uni-variate EN4 objective analyses from Met Office [Good et al. 2013] for temperature and salinity. The large-scale bias correction contributes positively to the reanalysis system by reducing the model drifts and systematic errors [Storto et al. 2015b].

3. Results

3.1 The Mean State and Variability of the North Atlantic Ocean

C-GLORS ocean reanalysis has been used in several studies [Cessi et al., 2014; Ezer 2015; Storto et al., 2015a]. However, this is the first time that this product is used to inspect the decadal-scale variability of the North Atlantic. In the present section, the mean state and variability over the North Atlantic region as reproduced by C-GLORS reanalysis are documented.

In Figure 1a the upper 500 m averaged temperature (T500) is shown for 1982-2013. The T500 climatological pattern displays a distinct meridional gradient across the Subtropical/Subpolar Gyre boundary, with a corresponding front located around 40°N.

Deep convection areas as identified by the march mixed layer depth (MMLD) proxy, mainly occur in the Labrador Sea (Figure 1b), where MMLD exceeds 800m, while a shallower 650m deep MMLD is found in the Irminger Seas. Labrador Sea convection is found in the northeast of the basin, in contrast with the Argo derived climatology from de Boyer Montegut et al. [2004] (not shown), indicating a relatively deeper convection (around 1000m) occurring in the south-western part of the Labrador Sea.

The mean 1982-2013 barotropic stream function averaged over the 1982-2013 period (Figure 1c) shows a cyclonic Subpolar Gyre circulation, with a 40 Sv strength close to observational estimates [Pickart et al., 2002]. Mesoscale variability is captured, especially in the western boundary of the subtropical regions.

The climatology of the AMOC from C-GLORS is shown in Figure 1d with the maximum of 17Sv located at 35°N. The monthly AMOC strength at 26°N, evaluated as the maximum meridional overturning streamfunction over the full water column, is shown in Figure 2a for both C-GLORS (black) and observations from Rapid-MOC (red). The mean AMOC at 26°N is 15.6 Sv, slightly weaker than the observed 17.2 Sv estimate obtained from the Rapid-MOC array [McCarthy et al., 2015]. For the 2005-2013 period (for which, C-GLORS and RAPID-MOC are directly comparable), the correlation between monthly observed and C-GLORS AMOC transport at 26° N is 0.82 (passing the 95% significance test). While this high correlation value is largely dictated by the seasonal cycle, it is worth noticing that the reanalysis is also able to capture some of the interannual and longer term fluctuations in the observed AMOC record, including the declining trend and the rapid drop in the AMOC strength that occurred on year 2010. After removal of the seasonal cycle from both C-GLORS and RAPID-MOC the correlation is still high (0.77, passing the 95% significance test). The monthly meridional heat transport (MHT) at 26°N for both C-GLORS (black) and observations (red, RAPID-MOCHA-MHT data derived from the RAPID-MOC array) is shown in Figure 2b. As for the AMOC, the correlation between monthly MHT in C-GLORS and observations is fairly large (0.85, passing the 95% significance test). Overall, we conclude that C-GLORS captures reasonably well the mean state and the variability of the North Atlantic Ocean.

3.2 The North Atlantic Warming in the mid-1990s

The evolution of T500 anomalies relative to the 1982-2013 climatology, time-averaged over different 5-year intervals encompassing the rapid warming event, is shown in Figure 3 (a-d). As expected, before 1995 a cold anomaly is well visible in the subpolar region, reaching its maximum during the 1991-1995 period. After 1996, the subpolar region starts to warm, reaching a maximum warming after 2001.

In concomitance with the SPG warming, the strength of the SPG cyclonic circulation strength (diagnosed through the barotropic streamfunction) decreases (Figure 4). Between 1991 and 1995 the SPG is particularly intense over the Labrador Sea but starts weakening after 1995 reaching its minimum strength in 2001-2005.

The year-to-year evolution of T500 anomalies computed with respect to the 1982-2013 baseline and basin-averaged over the subpolar region (50°N-66°N, 60°W-10°W, as shown in Figure 1a) is shown in Figure 5 (in black). From 1982 to 1995, T500 is cooler than normal and turns warmer after 1995. The temperature increment due to data assimilation, defined as the difference between analysis and background (model) temperatures is quantified. The temperature increment is the instantaneous value estimated every 7 days with the 3D-Var assimilation scheme. The contribution of data assimilation is therefore the accumulation over time of the 7-day increments. A negative (positive) increment indicates that data assimilation corrects a warm (cold)-

biased model state. Along with the area averaged T500 anomaly, the accumulation of temperature analysis increment in each year averaged in the same area is shown in Figure 5 (in orange). The mean negative temperature increments (-0.07) in Figure 5 suggest that the model has a warm bias (the minimum temperature increment reaches -0.47°C). The temperature field in the model is corrected by adding the temperature increment.

In order to fully establish the impact of data assimilation on the rapid warming event, we confronted the C-GLORS reanalysis with a twin control experiment, where only atmospheric fluxes are used to constrain the ocean state, but no assimilation (nor SST relaxation) is used. However, for the control run only the upper 700 m average temperature (T700) data had been retained, and therefore we could only assess the data assimilation impact for this specific diagnostic. From the comparison (not shown), it emerged that T700 is about 0.25C colder in C-GLORS than in the control run, confirming the (previously detected) warm bias affecting the dynamical ocean model. However, the control simulation appears to be able of correctly capturing the phase of the mid-90s warming. Thus, data assimilation is important to correct the model bias, but it is not crucial to reconstruct the time variability of the upper ocean temperature. However, due to the lack of additional information from the control simulation, it was not possible to perform a more comprehensive assessment of the impact of data assimilation (for instance, the impact on mass and heat transports).

3.3 Heat budget of the SPG region

Both changes in heat fluxes at the air-sea interface and heat transport convergence could be responsible for the detected warming in the SPG. In order to investigate the mechanism of the warming, the heat budget for the full depth in the SPG region is analyzed. We calculate variations of ocean heat content (OHC) at each monthly time step as follows:

$$\frac{\partial OHC}{\partial t} = \iint_{S_a} Q_{net} dxdy + Heat\ Transport\ Convergence\,(HTC) + Assimilation + residual$$

$$HTC = \rho_0 C_p \iint_{50N} TVdxdz + \rho_0 C_p \iint_{65N} TVdxdz + \rho_0 C_p \iint_{10W} TUdydz + \rho_0 C_p \iint_{60W} TUdydz$$

$$OHC = \rho_0 C_p \iiint_{S_o} Tdxdydz$$

,

where Q_{net} is the net (including latent and sensible heat fluxes, downward long- and short-wave radiation terms), U and V are zonal and meridional velocity , S_a is the area in the SPG region and S_0 is the ocean volume corresponding to the SPG region from the surface to the bottom. ρ_o and C_p are seawater density (1020 kg/m^3) and heat capacity (4000 J kg^{-1}C^{-1}) respectively. The first two terms that contribute to the heat budget are calculated following Barrier et al. [2015]. The first term on the right hand side of the equation represents the contribution to the OHC rate of change of surface heat fluxes, which is the surface integration of net surface heat fluxes in the SPG region. Positive values imply that the ocean gains heat from the atmosphere. The second term represents the contribution of heat transport convergence, which is the sum of the heat transport across all the sections (50°N, 66°N, 10°W and 60°W) that close the water volume in the SPG region. The temperature increment during the data assimilation process represented by T^a- T^b (with T^a and T^b the instantaneous analysis and background states respectively, estimated every 7 days with the 3D-Var assimilation scheme) contribute to the heat budget as well. We approximate the contribution of data assimilation to the heat budget as the heat content rate of change due to the temperature increment in the closed volume (the closed volume is the same as the volume in the calculation of total heat content). However, the precise calculation of the budget requires Qnet and HTC to be evaluated from T^b, rather than T, so as to correctlysingle out the contribution of assimilation (in fact, data assimilation does also indirectly affect Qnet and HTC through its impact on ocean circulations and SST). However, this is not possible in practice, leading to an approximate estimates of the heat budget terms. Additionally, the large-scale bias correction contributes to the heat budget as well, albeit difficult to quantify. We therefore prefer to include the assimilation contribution, given by the temperature increment during the data assimilation process and the large-scale correction, into the residuals term.

Figure 6 displays the individual terms of the OHC tendency equation. It is evident that the positive rate of change of OHC around 1995 is coherent with the heat transport convergence term. On the other hand, from 1993 to 1998 the surface heat fluxes decrease after 1997 (the ocean releases more heat to the atmosphere), suggesting that the surface heat fluxes do not contribute to the warming or weaken the warming signal. The correlation between monthly OHC rate of change and heat transport convergence (surface heat fluxes) computed over the 1982-2013 period using monthly data is 0.4 (0.29), increasing to 0.54 (0.38) if only the rapid warming transient period (1995-1999) is considered. The contribution of data assimilation plus residuals to the overall OHC rate of change is also shown in Figure 6. The mean contribution of data assimilation (not shown) is negative, indicating that the ocean state is systematically warmer than the analysis and the observations and the data assimilation process corrects this deficiency in the model behavior, which confirms the discussion above (negative temperature increment) that the model mean state has a warm bias.

Overall, the heat budget analysis confirms that the main contribution to the warming in the SPG comes from the heat transport convergence while surface heat fluxes plays a secondary role, in agreement with previous studies [Grist et al., 2010].

3.4 Meridional Heat transports

As mentioned above, ocean heat transport plays a major role in the warming of the SPG region. The heat transport convergence includes heat transport across lateral boundaries of the selected SPG box. The contribution of individual heat transport terms is shown in Figure 7. It is evident that the heat transport convergence variability is mainly due to the heat transport across the southern boundary (50°N in this study), while the overall transport across the meridional western and eastern boundaries plays a second order role.

Here we focus on the zonal transport across 50°N, analyzing the reasons for the detected increase of the heat transport. Following the approach outlined in Dong and Sutton [2002], the total heat transport is expressed in terms of time-mean and time-varying components, as follows. After splitting the meridional velocity and temperature fields into their mean and time-varying components, we obtain:

$$\rho_o C_p \int_{-H}^{0}\int_{\lambda_W}^{\lambda_E} VT dxdz = \rho_o C_p \int_{-H}^{0}\int_{\lambda_W}^{\lambda_E} \overline{V}\,\overline{T} dxdz + \rho_o C_p \int_{-H}^{0}\int_{\lambda_W}^{\lambda_E} V'\overline{T} dxdz$$
$$\rho_o C_p \int_{-H}^{0}\int_{\lambda_W}^{\lambda_E} \overline{V}T' dxdz + \rho_o C_p \int_{-H}^{0}\int_{\lambda_W}^{\lambda_E} V'T' dxdz,$$

where $\overline{v}$ and $\overline{T}$ are the 1982-2013 climatological values for the meridional velocity and temperature, v' and T' the corresponding anomalies relative to the annual climatology, λ_E (10°W) and λ_w (60°W) are the longitude of eastern and western boundaries of the ocean basin. At 50°N, both the anomalous advection of mean temperature and the mean advection of temperature anomalies (explaining 74% and

16% of the total variance, respectively) become relevant for the total heat transport, while the covariance of temperature and meridional circulation is negligible (Figure 8). In general, this result is consistent with previous studies [Msadek et al., 2014] indicating that the warming is mainly contributed by temporal fluctuations of meridional transport and advection of temperature anomalies. The major difference with respect to Robson et al. [2012a] findings is that in their case the anomalous advection of mean temperature term is important at 50°N and the covariance term becomes important after the rapid warming at 50°N. In our study, at 50°N the covariance term is negligible over most of the analyzed period. It is important to note that Robson et al. [2012a] use a model with a 2.4° spatial resolution, considerably coarser than the horizontal resolution used in C-GLORS.

The ocean circulation is commonly discussed separately in terms of gyre and meridional overturning circulation. In order to distinguish the relative contributions to the total heat transport associated with the gyre circulation and meridional overturning circulation, a more dynamically insightful characterization of the heat transport, based on the method developed by Bryden and Imawaki [2001] is provided. The component of the heat transport across the 50°N zonal transoceanic section due to the AMOC, Q_{amoc}, is defined as:

$$Q_{amoc} = \rho_0 C_p \int <v(z)><T(z)> L(z) dz$$

where $<v(z)>$ and $<T(z)>$ are zonally-averaged velocity and temperature at each depth and $L(z)$ is the width of the section at each depth. The component of the heat transport due to the gyre circulation (Q_{gyre}) is defined as:

$$Q_{gyre} = \iint \rho_0 C_p v(x,z)' T(x,z)' dx dz$$

where v' and T' are deviations from the zonal averages.

The temporal variability of these two components across 50°N is shown in Figure 9. During the rapid warming period, from 1995 to 1999, both AMOC and gyre circulation components increase. However, the relative increase of Q_{gyre} during the warming transient is larger than Q_{amoc}. Also, it is seen that Q_{gyre} has a longer temporal persistence through the whole warming period, while Q_{amoc}, shows a rapid decay after year 1995. The important role found for the gyre circulation over the total zonal heat transport across 50N, is consistent with Grist et al. [2010]. By using an eddy-permitting ocean model without data assimilation, they show that from 50°N to 65°N the mean heat transport can be largely ascribed to the gyre component.

4. Summary and Conclusions

An eddy-permitting ocean reanalysis is used to analyze the rapid warming observed in the Subpolar Gyre region in the mid-1990s. In general, the ocean reanalysis realistically captures the mean state and variability of the North Atlantic Ocean. Consistent with existing observations, the T500 evolution reproduces the sharp increase around year 1995, particularly pronounced over the eastern subpolar region and western part of the Labrador Sea. After year 2000 the warming affects the whole subpolar region. The rapid warming appears to be associated with a weakening of the Subpolar Gyre circulation consistent with existing observations and model-based analyses. An analysis of the temperature increments introduced by the data assimilation process and a comparison between C-GLORS and a control, purely forced, hindcast simulation reveals that the assimilation contributes to correct the bias in the model background state, but its impact on the phase of the mid-90s SPG warming is relatively small. The heat budget in the SPG region (50°N-66°N, 60°W-10°W) indicates that the detected mid-1990s warming is mainly due to the increase of heat transport convergence with a 0.54(0.38) correlation between OHC rate of change and heat transport convergence (surface heat fluxes) during the 1995 to 1999 warming transient, consistent with a previous study by Grist et al. [2010].

The increase of the heat transport convergence in the SPG region mainly comes from the heat transport across the southern boundary (50°N in this study). A more detailed analysis demonstrates that the total heat transport is mainly contributed by both the anomalous advection of mean temperature and the mean advection of temperature anomalies, consistent with Msadek et al. [2014]. In order to gain a better dynamical insight of the processes driving the heat transport variability, we calculate the AMOC and gyre circulation components of the heat transport across 50°N following Bryden and Imawaki [2001]. The result shows that both AMOC and gyre circulation contribute to the increase of the heat transport, with a prominent role played by gyre circulation as discussed in [Grist et al., 2010; Msadek et al., 2014].

Previous studies have debated on the role played by the NAO on the mid-1990s SPG warming [Robson et al., 2012a, Lohmann et al., 2009a; Herbaut and Houssais, 2009; Häkkinen et al., 2011]. Figure 10 displays several normalized indices. These include the AMOC transport at 50°N, barotropic streamfunction (sign-reversed) and T500 area-averaged over the SPG region, two indices for the meridional heat transport at 50°N (split into gyre and AMOC components) and the NAO index. It appears that the meridional heat transport increase is accompanied with the strengthening of ocean circulation. The strengthening of ocean circulation may be the response to the positive NAO, as proposed by Robson et al. [2012]. In order to further explore the relationship between NAO and ocean circulation we regress the annual mean meridional overturning and barotropic streamfunctions onto the DJFM NAO index (Figure 11 and Figure 12).

The AMOC adjustment to NAO interannual changes reveals a fast, basin-wide response, with a local peak in the subtropics at lag-zero, followed by a lagged high-latitude response, possibly associated with the intensification of the overturning circulation determined by NAO-induced dense water formation pulses in the subpolar basin. This is further corroborated by hints of southward propagation of AMOC transport anomalies, evident at time-lags 3-to-5 years, a typical signature of the Deep Western Boundary Current delayed adjustment following the generation of dense waters in the Labrador basin. Interestingly, these results bear some resemblance with the analysis performed by Kwon and Frankignoul [2012)] and Barrier et al. [2014].

The barotropic streamfunction (shown in figure 12) exhibits a zero-lag response characterized by an anomalous anticyclonic circulation at the inter-gyre boundary, followed by a delayed intensification of the western Subpolar Gyre cyclonic circulation, reaching its peak 2 years later. This is consistent with previous analyses on the impact of the NAO on the barotropic circulation [Marshall et al., 2001; Barrier et al., 2013; Bellucci et al., 2008]. Marshall and co-workers [2001] in particular suggested that a positive NAO phase induces an anticyclonic gyre circulation at the Subtropical/Subpolar Gyre boundary (the so called, “inter-gyre gyre”) associated with a poleward shift of the North Atlantic Current pathway [see also Fig. 6 in Barrier et al., 2014].

To summarize, our results suggest that both the barotropic and the overturning circulation play a role in the observed changes of the SPG upper ocean temperatures. In particular the barotropic circulation zero-lagged response to changes in the phase of the NAO (through the inter-gyre gyre circulation) appears to be consistent with the cross-gyre anomalous transport of mean temperature ($v'\overline{T}$), while the slowly evolving AMOC, relatively less sensitive to abrupt, interannual variations in the NAO phase, feeds the large-scale advection of thermal anomalies across 50°N ($\bar{v}T'$; Fig. 8). The persistently positive phase of the NAO during the years prior to the rapid warming, did likely favour the poleward heat transfer, and the following SPG warming, consistent with the mechanism outlined in Msadek et al. [2014].

Acknowledgements:

The authors are grateful to the three anonymous reviewers and the editor for their very detailed and helpful comments. This research is funded by Italian national project GEMINA.

5. References:

Barnier B., G. Madec, T. Penduff, J. M. Molines, A. M. Treguier, J. Le Sommer, J. Beckmann, C. Boning, J. Dengg, D. Derval, C. Durand, S. Gulev, E. Remy, C. Talandier, S. Theeren, M. Maltrud, J. McClean and B. De Cuevas, 2006: Impact of partial steps and momentum advection schemes in a global ocean circulation model at eddy-permitting resolution. *Ocean Dynamics*, **56**, 543-567, doi: 10.1007/s10236-006-0082-1.

Barrier, N., C. Cassou, J. Deshayes and A-M Treguier, 2014, Response of North Atlantic Ocean Circulation to Atmospheric Weather Regimes. *J. Phys. Oceanogr.*, **44**, 179-201.

Barrier, N., J. Deshayes, A. Treguier and C. Cassou, 2015: Heat budget in the North Atlantic Subpolar Gyre: Impacts of atmospheric weather regimes on the 1995 warming event. *Progress in Oceanography,* **130**, 75-90, doi:10.1016/j.pocean.2014.10.001.

Bersch, M., I . Yashayaev and K. P. Koltermann, 2007: Recent changes of the thermohaline circulation in the subpolar North Atlantic. *Ocean Dynamics*, **57**, 223-235.

Bellucci, A. and K.J. Richards, 2006: Effects of NAO variability on the North Atlantic Ocean circulation, *Geophysical Research Letters*, **33**, L02612.DOI:10.1029/2005GL024890

Bellucci, A.**,** S. Gualdi, E. Scoccimarro and A. Navarra, 2008: NAO-ocean interactions in a coupled general circulation model, *Climate Dynamics*, **31**, 759-777, DOI 10.1007/s00382-008-0408-4.

Brauch, J. P. and R. Gerdes, 2005: Response of the northern North Atlantic and Arctic oceans to a sudden change of the North Atlantic Oscillation. *J. Geophys. Res.*, **110**, C11018, doi: 10.1029/2004JC002436.

Bryden, H. L. and S. Imawaki, 2001: Ocean heat transport. In Ocean Circulation and Climate. G. Siedler, J. Church and J. Gould, Eds., Academic Press, *International Geophysics Series*, 77, 453-521.

Cavalieri, D., D. Parkinson, P. Gloersen and H. J. Zwally, 1996: Sea ice concentrations from Nimbus-7 SMMR and DMSP SSM/I-SSMIS passive Microwave data. Boulder, Colorado, USA: NASA DAAC at the National Snow and Ice Data Center.

Cessi, P., N. Pinardi and V. Lyubartsev, 2014: Energetics of semienclosed basins with two-layer flows at the Strait. *J. Phys. Oceanogr*., **44,** 967-979, doi; sx.soi.og/10.1175/JPO-D-13-0129.1

Dai. A and K. E. Trenberth, 2002: Estimates of freshwater discharge from continents: Latitudinal and seasonal variations. *J. Hydrometeor*, **3**, 660-687.

Dee, D. P., S. M. Uppala, A. J. Simmons, P. Berrisford, P. Poli, S. Kobayashi, U. Andrae, M. A. Balmaseda, G. Balsamo, P. Bauer, P. Bechtold, A. C. M. Beljaars, L. van de Berg, J. Bidlot, N. Bormann, C. Delsol, R. Dragani, M. Fuentes, A. J. Geer, L. Haimberger, S. B. Healy, H. Hersbach, E. V. Hólm, L. Isaksen, P. Kållberg, M. Köhler, M. Matricardi, A. P. McNally, B. M. Monge-Sanz, J.-J. Morcrette, B. –K. Park, C. Peubey, P. de Rosnay, C. Tavolato, J. –N. Thépaut and F. Vitart, 2011: The ERA-Interim reanalysis: Configuration and performance of the data assimilation system. *Q. J. R. Meterol. Soc*, **137,** 553-597.

Desbruyères, D., H. Mercier and V. Thierry, 2014: On the mechanisms behind decadal heat content changes in the eastern Subpolar Gyre. *Progress in Oceanography*, In press, doi: 10.1016/j.pocean.2014.02.005.

Dommenget, D. and M. Latif, 2000: Interannual to decadal variability in the tropical Atlantic. *J. Climate*, **13**, 777-792.

Dong, B and R. T. Sutton, 2002: Variability in North Atlantic heat content and heat transport in a coupled ocean-atmosphere GCM. *Climate Dynamics*, **19**, 485-497.

Eden, D., and J. Willebrand, 2001: Mechanism of interannual to decadal variability of the North Atlantic circulation. *J. Climate*, **14**, 2266-2280.

Ezer, T., 2015: Detecting changes in the transport of the Gulf Stream and the Atlantic overturning circulation from coastal sea level data: The extreme decline in 2009-2010 and estimated variations for 1935-2012. *Global and Planetary Change,* **129**, 23-26.

Fichefet, T and M. A. Morales Maqueda, 1997: Sensitivity of a global sea ice model to the treatment of ice thermodynamics and dynamics. J. *Geophys. Res*., **102**, 12609-12646.

Grist, J. P., S. A. Josey, R. Marsh, A. A. Good, A. C. Coward, B. A. de Cuevas, S. G. Alderson, A. L. New and G. Madec, 2010: The roles of surface heat flux and ocean heat transport convergence in determining Atlantic Ocean temperature variability. *Ocean Dynamics*, **60**, 771-790, doi: 10.1007/s10236-010-0292-4.

Häkkinen, S and P. B. Rhines, 2004: Decline of subpolar North Atlantic circulation during the 1990s. *Science*, **304,** 555-559, doi: 10.1126/science.1094917.

Häkkinen, S, P. B. Rhines and D. L. Worthen, 2011: Warm and saline events embedded in the meridional circulation of the northern North Atlantic. *J. Geophys. Res*, **116,** C03006.

Hátún, H., A. B. Sando, H. Drange, B. Hansen and H. Valdimarsson, 2005: Influence of the Atlantic Subpolar Gyre on the thermohaline circulation. *Science*, **309**, 1841-1844, doi: 10.1126/science.1114777.

Hátún, H, M. R. Payne and J. A. Jacobsen, 2009: The North Atlantic Subpolar Gyre regulates the spawning distribution of blue whiting (Micromesistius poutassou). *Canadian Journal of Fisheries and Aquatic Sciences*, **66**, 759-770, doi: 10.1139/F09-037.

Herbaut, C. and M. N. Houssais, 2009: Response of the eastern North Atlantic Subpolar Gyre to the North Atlantic Oscillation. *Geophy. Res. Lett*, **36**, L17607, doi: 10.1029/2009GL039090.

Holland, D. M., R. H. Thomas, B. de young, M. H. Ribergaard and B. Lyberth, 2008: Acceleration of Jakobshavn Isbrae triggered by warm subsurface ocean waters. *Nature Geoscience*, **1**, 659-664, doi: 10.1038/ngeo316.

Hurrell, J. W. and C. Deser, 2009: North Atlantic climate variability: The role of the North Atlantic Oscillation. *J. Marine System*, **79**, 231-244.

Ingleby, B. and M. Huddleston, 2007: Quality control of ocean temperature and salinity profiles – historical and real-time data. *J. Mar. Syst*., **65,** 158-175.

Johns, W., M. O. Baringer, L. M. Beal, S. A. Cunningham, T. Kansow, H. L. Bryden, J. J. M. Hirschi, J. Marotzke, C. S. Meinen, B. Shaw and R. Curry, 2011: Continuous, array-based estimates of Atlantic Ocean heat transport at 26.5°N. *J. Climate*, **24**, 2429-2449.

Kushnir, Y., 1994: Interdecadal variations in North-Atlantic sea surface temperature and associated atmospheric conditions. *J. Climate*, **7**, 141-157.

Kwon Y., C. Frankignoul 2012: Stochastically driven multidecadal variability of the Atlantic meridional overturning circulation in CCSM3, *Clim. Dyn.*, **38,** 859-876.

Large, W. G. and S. G. Yeager, 2004: Diurnal to decadal global forcing for ocean and sea ice models: the data sets and flux climatologies. *Technical report No.460*, NCAR Technical Note.

Lohmann, K., H. Drange and M. Bentsen, 2009a: Response of the North Atlantic Subpolar Gyre to persistent North Atlantic Oscillation like forcing. *Climate Dynamics*, **32**, 273-285, doi:10.1007/s00382-008-0467-6.

Lohmann, K., H. Drange and M. Bentsen, 2009b: A possible mechanism for the strong weakening of the North Atlantic Subpolar Gyre in the mid-1990s. *Geophy. Res. Lett.*, **36**, L15602, doi:10.1029/2009GL039166.

Madec, G., P. Delecluse, M. Imbard and C. Levy, 1998: OPA 8 ocean general circulation model – reference manual. *Tech. rep., LODYC/IPSL Note 11.*

Marsh, R., S. A. Josey, B. A. de Cuevas, L. J. Redbourn and G. D. Quartly, 2008: Mechanisms for recent warming of the North Atlantic: Insights gained with an eddy-permitting model. *J. Geophys. Res*., **113**, C04031, doi: 10.1029/2007JC004096.

Marshall, J., H. Johnson and J. Goodman, 2001, A study of the interaction of the North Atlantic Oscillation with ocean circulation. *J. Climate,* **14**, 1399-1421.

McCarthy, G. D., D. A. Smeed, W. E. Hohns, E. Frajka-Williams, B. I. Moat, D. Rayner, M. O. Bariner, C. S. Meinen, J. Collins and H. L. Bryden, 2015: Measuring the Atlantic Meridional Overturning Circulation at 26°N. *Progress in Oceanography*, **130**, 91-111.

McGregor S, A. Timmermann, M. F. Stuecker, M. H. England, M. Merrifield, Fei-Fei Jin and Y. Chikamoto, 2014: Recent walker circulation strengthening and Pacific cooling amplified by Atlantic warming. *Nature Climate Change*, **4**, 888-892, doi: 10.1038/NCLIMATE2330.

Msadek, R, T. L. Delworth, A. Rosati, W. Anderson, G. Vecchi, Y. S. Chang, K. Dixon, R. G. Gudgel, W. Stern, A. Wittenberg, S. Yang, F. Zeng, R. Zhang and S. Zhang, 2014: Prediction a decadal shift in North Atlantic climate variability using the GFDL forecast system. *J. Climate*, **27**, 6472-6496.

Pickart, R. S., D. J. Torres and R. A. Clarke, 2002: Hydrography of the Labrador Sea during active convection. *J. Phys. Oceanogr.*, **32**, 428-457.

Reynolds, R. W., T. M. Smith, C. Liu, D. B. Chelton, K. S. Casey and M. G. Schlax, 2007: Daily high-resolution blended analyses for sea surface temperature. *J. Climate,* **20,** 5473-5496.

Robson, J., R. Sutton, K. Lohmann, D. Smith and M. D. Palmer, 2012a: Causes of the rapid warming of the North Atlantic Ocean in the mid-1990s. *J. Climate*, **25,** 4116-4134, doi: 10.1175/JCLI-D-11-00443.1.

Robson, J. I., R. T. Sutton and D. M. Smith, 2012b: Initialized decadal predictions of the rapid warming of the North Atlantic Ocean in the mid 1990s. *Geophy. Res. Lett*, **39,** L19713, doi: 10.1029/2012GL053370.

Sarafanov, A., A. Falina, A. Solov and A. Demidov, 2008: Intense warming and salinification of intermediate waters of southern origin in the eastern subpolar North Atlantic in the 1990s to mid-2000s. *J. Geophys. Res*., **113**, C12022, doi: 10.1029/2008JC004975.

Smith D. M., R. Eade, N. J. Dunstone, D. Fereday, J. M. Murphy, H. Pohlmann and A. A. Scife, 2010: Skilful multi-year predictions of Atlantic hurricane frequency. *Nature Geoscience*, **3,** 846-849, doi: 10.1038/NGEO1004.

Storto, A., S. Masina, M. Balmaseda, S. Guinehut, Y. Xue, T. Szekely, I. Fukumori, G. Forget, Y-S. Chang, S. A. Good, A. Kohl, G. Vernieres, N. Ferry, K. A. Peterson, D. Behringer, M. Ishii, S. Masuda, Y. Fujii, T. Toyoda, Y. Yin, M. Valdivieso, B. Barnier, T. Boyer, T. Lee, J. Gourrion, O. Wang, P. Heimback, A. Rosati, R. Kovach, F. Hernandez, M. J. Martin, M. Kamachi, T. Kuragano, K. Mogensen, O. Alves, K. Haines, X. Wang, 2015: Steric sea level variability (1993-2010) in an ensemble of ocean reanalyses and objective analyses. *Climate Dynamics*, published online, doi: 10.1007/s00382-015-2554-9.

Storto, A., S. Masina and A. Navarra, 2015b: Evaluation of the CMCC eddy-permitting global ocean physical reanalysis system (C-GLORS, 1982-2012) and its assimilation. Accepted, *Quart. J. Royal. Meteo. Soc*. Doi: 10.1002/qj.2673.

Storto, A, S. Masina and S. Dobricic, 2014: Estimation and impact of non-uniform horizontal correlation length scales for global ocean physical analyses. *J. Atmos, Oceanic. Technol.*, **31**, 2330-2349.

Storto A., S. Dobricic, S. Masina and P. Di Pietro, 2011: Assimilating along-track altimetric observations throught local hydrostatic adjustments in a global ocean reanalysis system. *Mon. Wea. Rev*., **139**, 738-754.

Sutton, R. T. and D. L. R. Hodson, 2003: Influence of the ocean on North Atlantic climate variability 1871-1999. *J. Climate*, **16**, 3296-3313.

Sutton, R. T. and D. L. R. Hodson, 2005: Atlantic Ocean forcing of North American and European summer climate. *Science*, **309**, 115-118, doi: 10.1126/science.1109496.

Sutton, R. T. and B. Dong, 2012: Atlantic Ocean influence on a shift in European climate in the 1990s. *Nature Geoscience*, **5**, *788-792*, doi: 10.1038/NGEO1595.

Thierry, E. de Boisseson, H. Mercier, 2008: Interannual variability of the subppolar mode water properties over the Reykjanes ridge during 1990-2006, *J. Geophys. Res.: Oceans*, **113**, C04016.

Ting M., Y. Kushnir, R. Seager and C. Li, 2009: Forced and internal Twentieth Century SST trends in the North Atlantic. *J. Climate*, **22,** 1469-1481.

Visbeck, M., E. Chassignet, R. Curry, T. Delworth, B. Dickson and G. Krahmann, 2003: The ocean's response to North Atlantic Oscillation variability. The North Atlantic Oscillation: Cinematic Significance and Environmental Impact. *Geophys. Monogr.*, Vol. **134**, Amer. Geophys., Union, 113-146.

Wijffels, S. E, J. Willis, C. M. Domingues, P. Barker, N. J. White, A. Gronell, K. Ridgway and J. A. Church, 2008: Changing expendable bathythermograph fall rates and their impact on estimates of thermosteric sea level rise. *J. Climate*, **21**, 5657-5672.

Yeager, S., A. Karspeck, G. Danabasoglu, J. Tribbia and H. Teng, 2012: A decadal prediction case study: Late Twentieth-Century North Atlantic ocean heat content. *J. Climate*, **25**, 5173-5189, doi:10.1175/JCLI-D-11-00595.1.

Zalesak, S. T., 1979: Fully multidimensional flux corrected transport algorithms for fluid. *J. Computer. Phys.*, **31**, 335-362.

Figures Captions

Figure 1. Mean state of C-GLORS ocean reanalysis for (a) T500 (°C), (b) March mixed layer depth (m), (c) barotropic streamfunction (Sv), and (d) AMOC (Sv) for the1982–2013 period.

Figure 2. a) Maximum AMOC strength at 26°N, (Sv), and b) meridional heat transport across 26°N (PW) for C-GLORS reanalysis (black) and RAPID array observations (red).

Figure 3. T500 anomalies (°C) relative to the 1982-2013 climatology averaged over pentads (a) 1986-1990, (b) 1991-1995, (c) 1996-2000, and (d) 2001-2005.

Figure 4. Barotropic streamfunction anomalies (Sv) relative to the 1982-2013 climatology averaged over pentads (a) 1986-1990, (b) 1991-1995, (c) 1996-2000, and (d) 2001-2005.

Figure 5. Area averaged T500 anomaly (°C) in black and the time accumulation temperature increment during each year (representing the contribution of temperature increment to the temperature field) in orange in the SPG region (50°N-66°N, 60°W-10°W).

Figure 6. Heat budget in the SPG region. The rate of change of ocean heat content is in black; the contribution from heat transport convergence is in blue; the contribution from integrated surface heat fluxes is in red; the sum of the approximation of the contribution from data assimilation, large bias correction and the residual is in green. Dashed lines are the long-term mean values.

Figure 7. Heat transport convergence in the SPG region and heat transport across the Northern (63°N), Southern (50°N), and Western-Eastern boundaries in the SPG region (PW).

Figure 8. Components of annual mean meridional heat transport (in PW) across 50°N in the SPG region due to anomalous advection of time-mean temperature ($v'\overline{T}$, in red), advection of temperature anomalies from time-mean circulation ($\overline{v}T'$, in green), and the covariance between velocity and temperature anomalies ($v'T'$, in blue). The sum of the three components is shown in black.

Figure 9. Meridional heat transport anomaly (PW) across 50°N in the SPG region due to the AMOC (in red), and gyre circulation component (in blue).

Figure 10. Normalized winter (DJFM NAO index; dashed black), barotropic stream function anomaly (sign-reversed) and T500 anomaly basin-averaged over the SPG region (dashed blue and solid black respectively), the AMOC mass transport at 50°N (dashed red) the heat transport across 50°N contributed by the AMOC (solid red) and gyre circulation (solid blue). All values are normalized. The NAO index is from https://climatedataguide.ucar.edu/climate-data/hurrell-north-atlantic-oscillation-nao-index-station-based

Figure 11 Linear regression coefficient of annual mean Atlantic meridional overturning streamfunction onto the winter NAO index at time-lags 0-5 years (in Sv per unit change in NAO index). NAO index leads for positive time-lags. The mean state of the AMOC from 1982-2013 is in contours. Areas that pass 95% significant values are shown in dots.

Figure 12 Linear regression coefficient of annual mean barotropic streamfunction onto the winter NAO index at time-lags 0-4 years (in Sv per unit change in NAO index) in shaded. The NAO index leads for positive time-lags. The mean state of the barotropic streamfunction from 1982-2013 is in contours. Areas that pass 95% significant values are shown in dots.

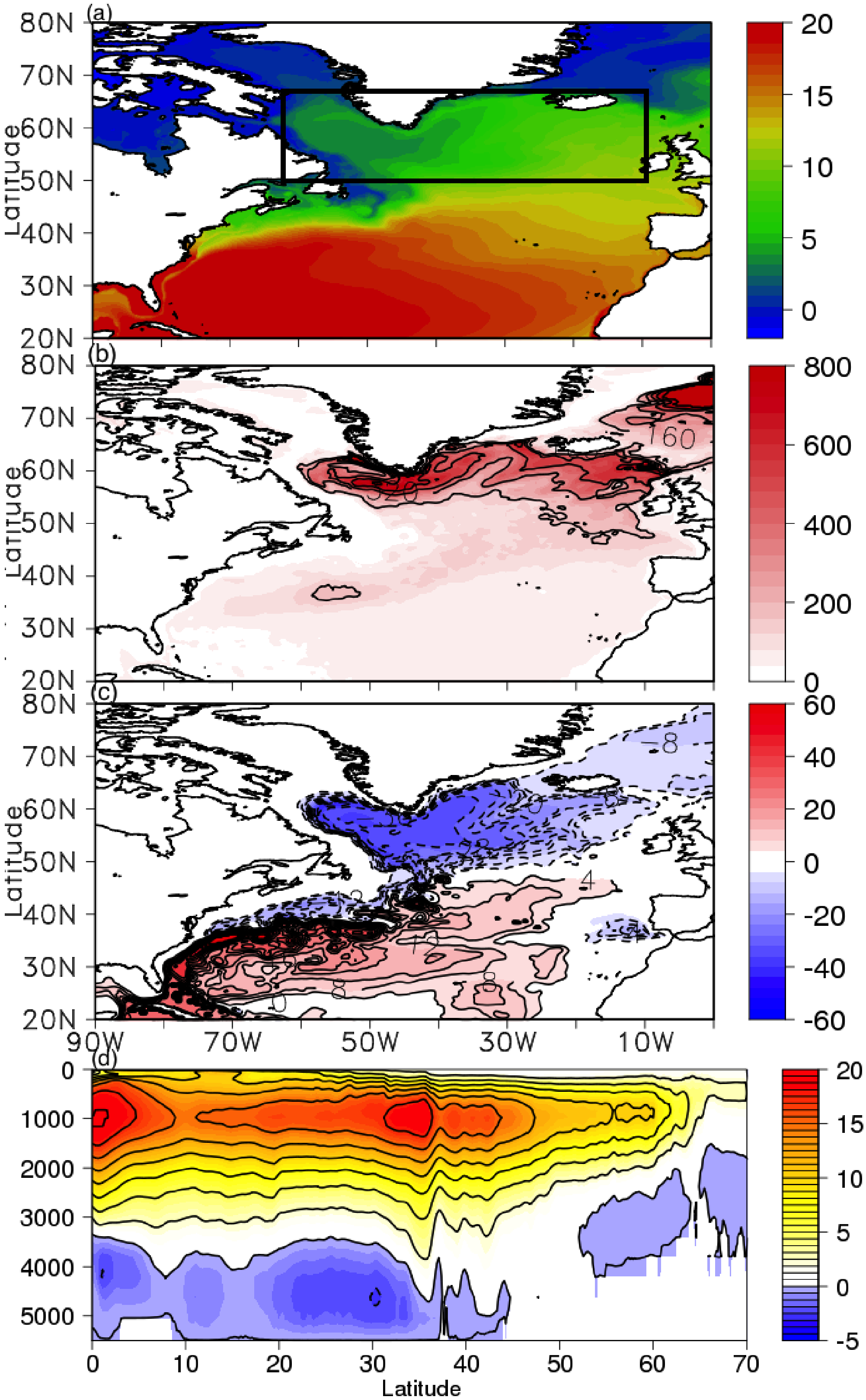

Figure 1. Mean state of C-GLORS ocean reanalysis for (a) T500 (°C), (b) March mixed layer depth (m), (c) barotropic streamfunction (Sv), and (d) AMOC (Sv) for the1982–2013 period.

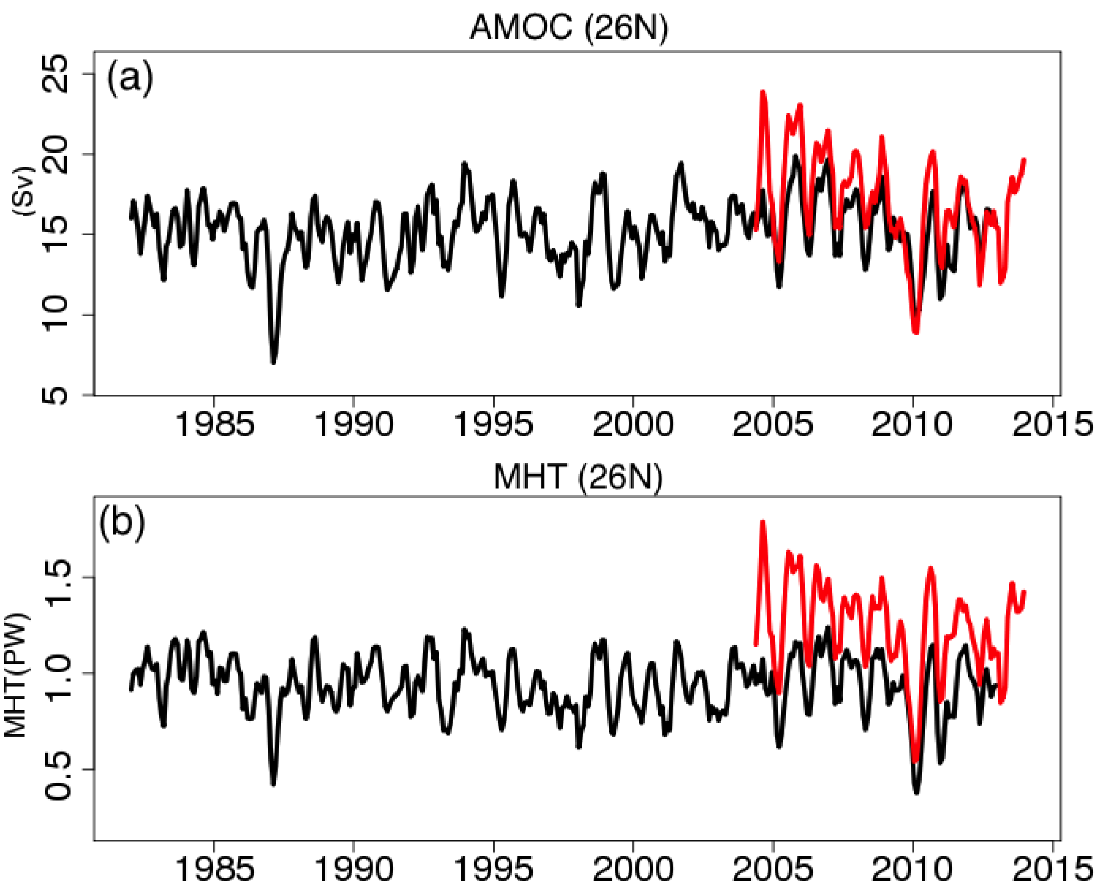

Figure 2. a) Maximum AMOC strength at 26°N, (Sv), and b) meridional heat transport across 26°N (PW) for C-GLORS reanalysis (black) and RAPID array observations (red).

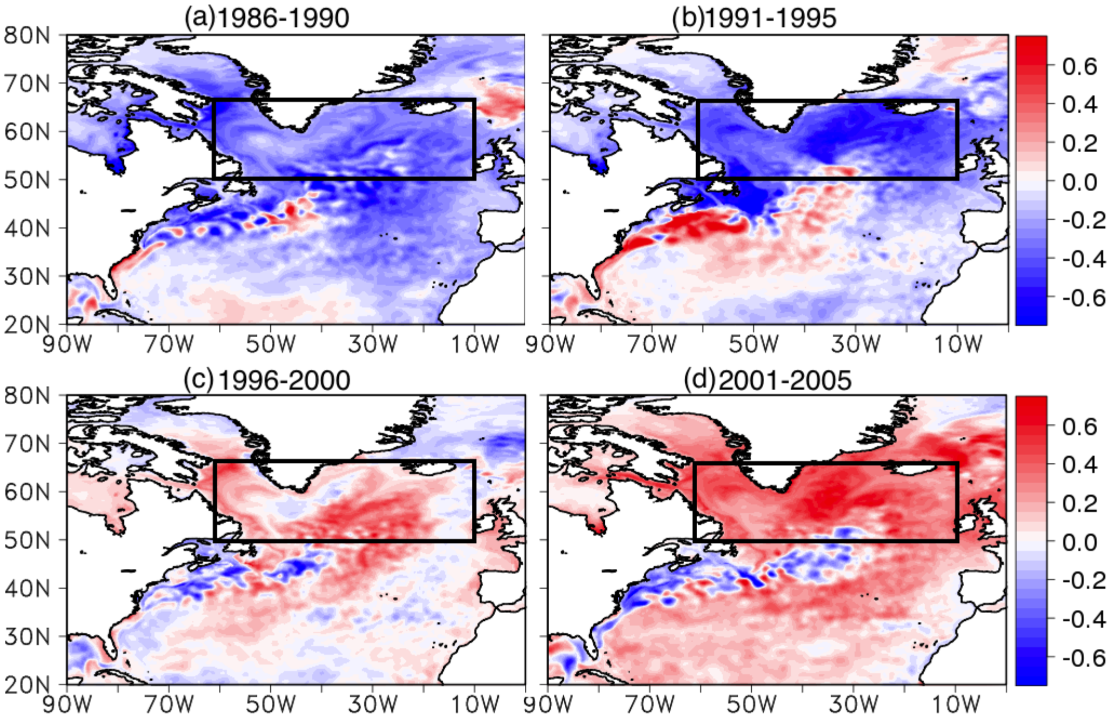

Figure 3. T500 anomalies (°C) relative to the 1982-2013 climatology averaged over pentads (a) 1986-1990, (b) 1991-1995, (c) 1996-2000, and (d) 2001-2005.

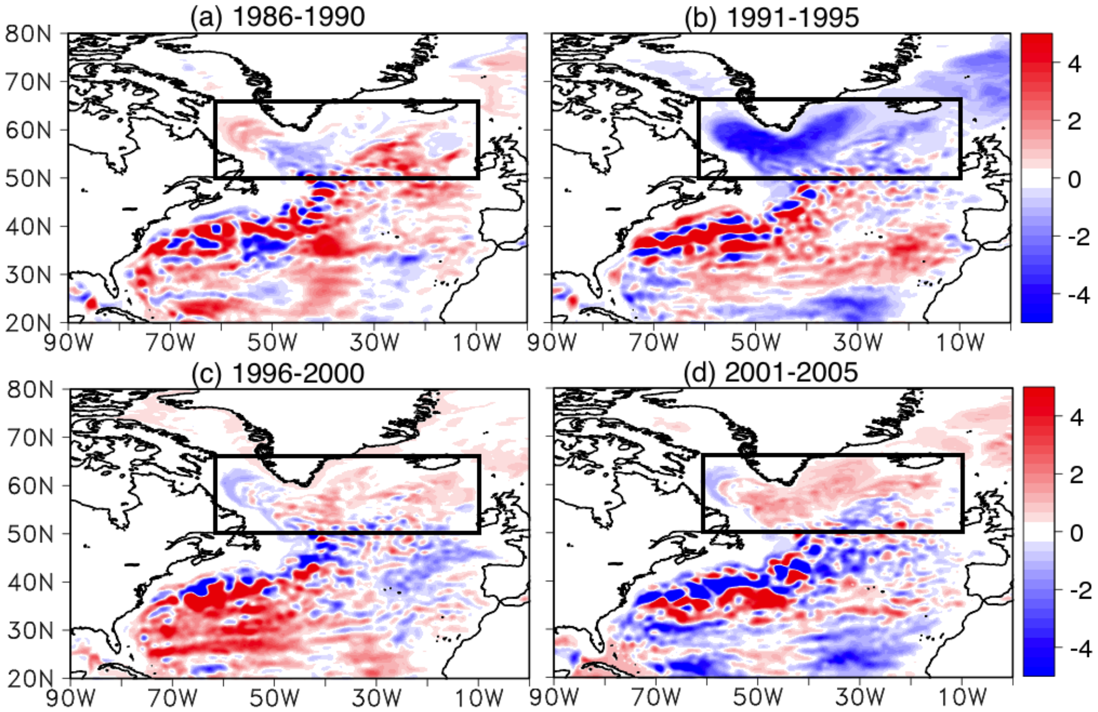

Figure 4. Barotropic streamfunction anomalies (Sv) relative to the 1982-2013 climatology averaged over pentads (a) 1986-1990, (b) 1991-1995, (c) 1996-2000, and (d) 2001-2005.

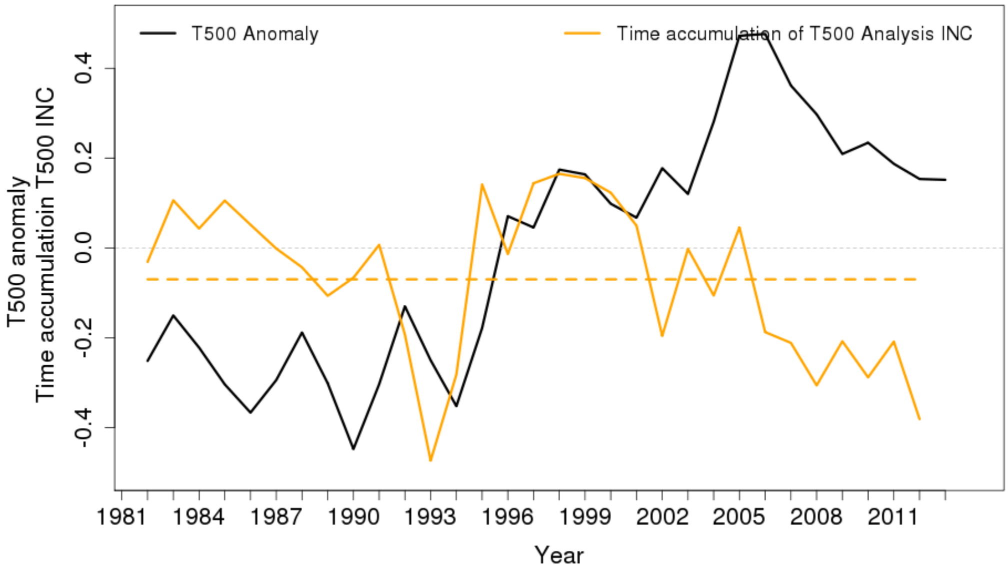

Figure 5. Area averaged T500 anomaly (°C) in black and the time accumulation temperature increment during each year (representing the contribution of temperature increment to the temperature field) in orange in the SPG region (50°N-66°N, 60°W-10°W).

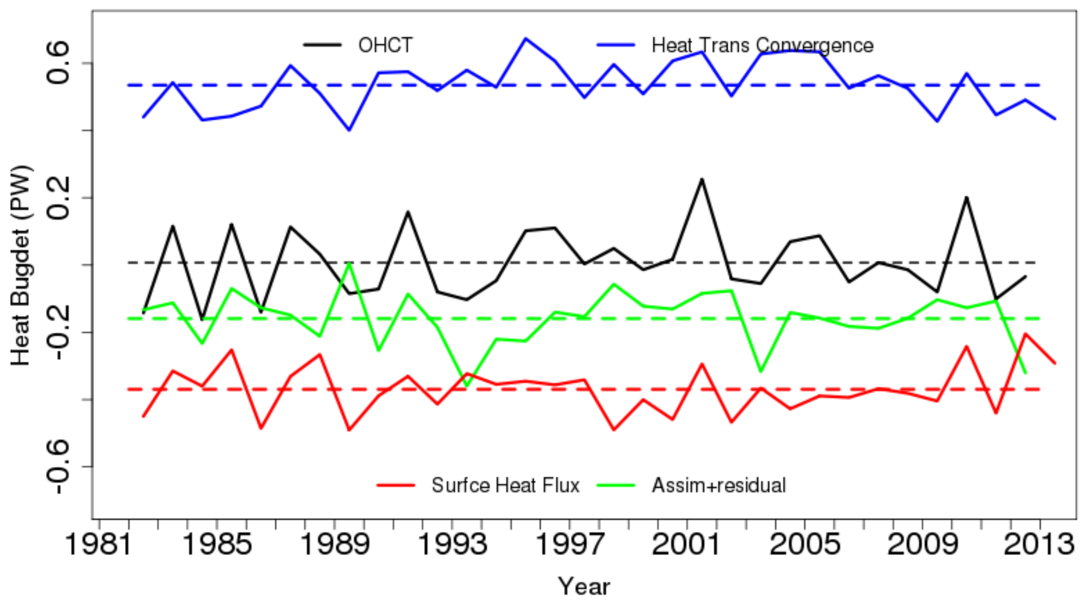

Figure 6. Heat budget in the SPG region. The rate of change of ocean heat content is in black; the contribution from heat transport convergence is in blue; the contribution from integrated surface heat fluxes is in red; the sum of the approximation of the contribution from data assimilation, large bias correction and the residual is in green. Dashed lines are the long-term mean values.

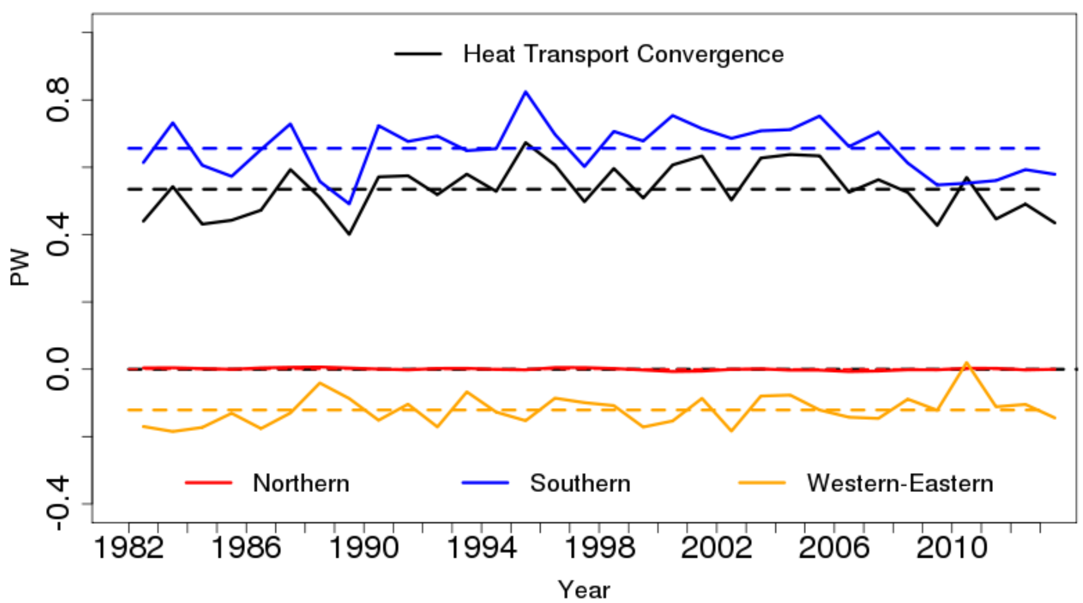

Figure 7. Heat transport convergence in the SPG region and heat transport across the Northern (63°N), Southern (50°N), and Western-Eastern boundaries in the SPG region (PW).

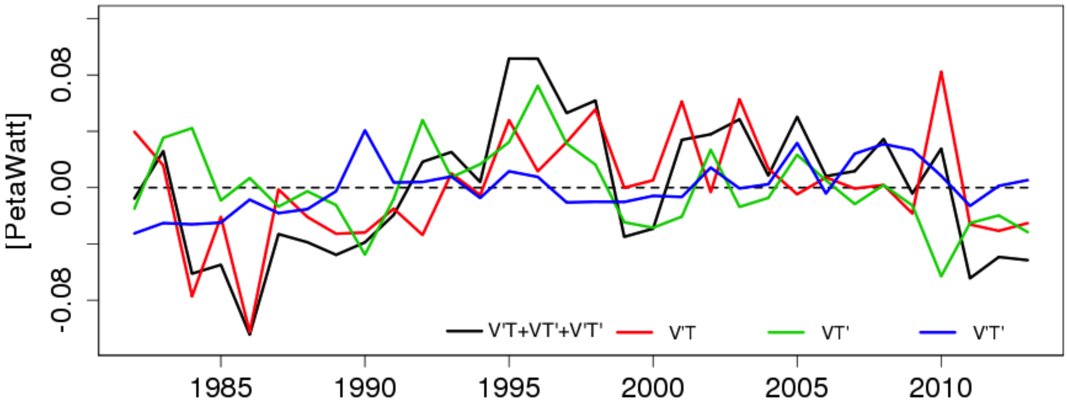

Figure 8. Components of annual mean meridional heat transport (in PW) across 50°N in the SPG region due to anomalous advection of time-mean temperature ($v'\overline{T}$, in red), advection of temperature anomalies from time-mean circulation ($\overline{v}T'$, in green), and the covariance between velocity and temperature anomalies ($v'T'$, in blue). The sum of the three components is shown in black.

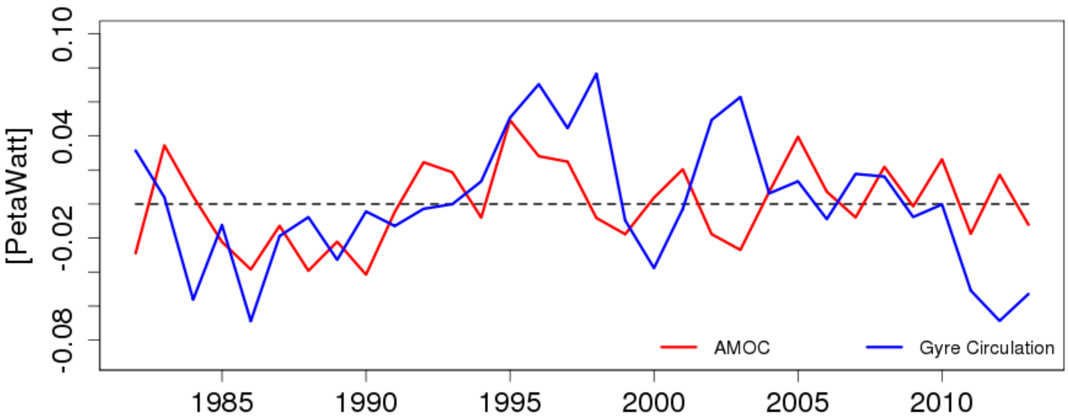

Figure 9. Meridional heat transport anomaly (PW) across 50°N in the SPG region due to the AMOC (in red), and gyre circulation component (in blue).

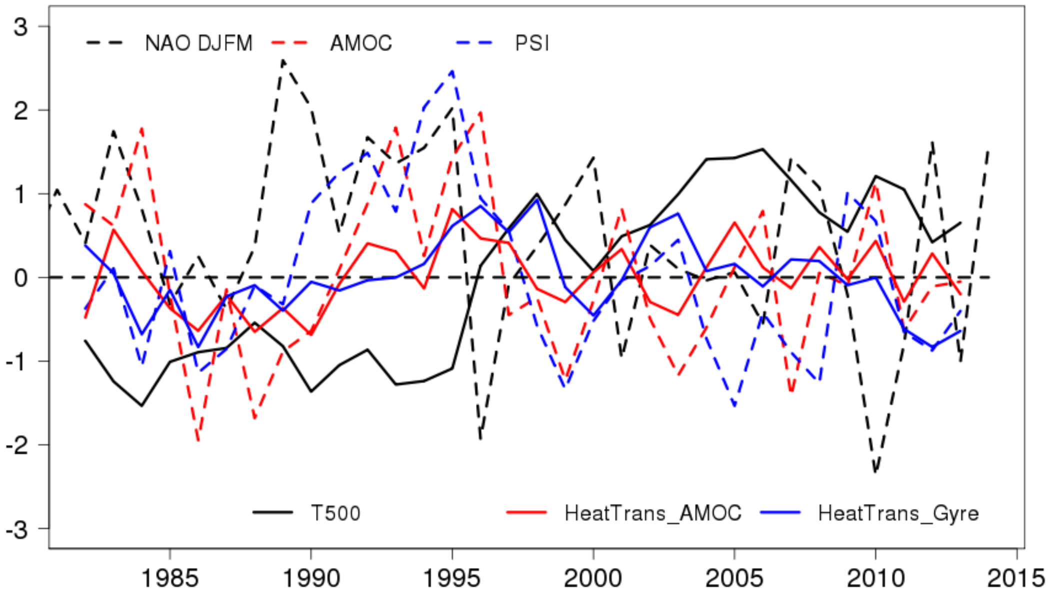

Figure 10. Normalized winter (DJFM NAO index; dashed black), barotropic stream function anomaly (sign-reversed) and T500 anomaly basin-averaged over the SPG region (dashed blue and solid black respectively), the AMOC mass transport at 50°N (dashed red) the heat transport across 50°N contributed by the AMOC (solid red) and gyre circulation (solid blue). All values are normalized. The NAO index is from https://climatedataguide.ucar.edu/climate-data/hurrell-north-atlantic-oscillation-nao-index-station-based

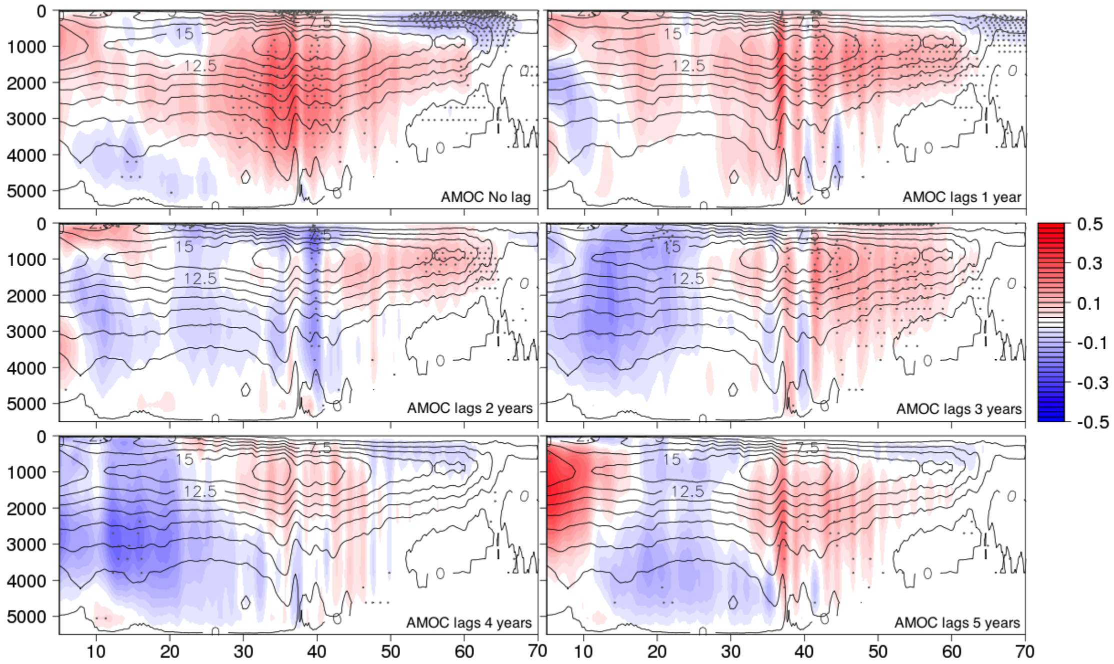

Figure 11 Linear regression coefficient of annual mean Atlantic meridional overturning streamfunction onto the winter NAO index at time-lags 0-5 years (in Sv per unit change in NAO index). NAO index leads for positive time-lags. The mean state of the AMOC from 1982-2013 is in contours. Areas that pass 95% significant values are shown in dots.

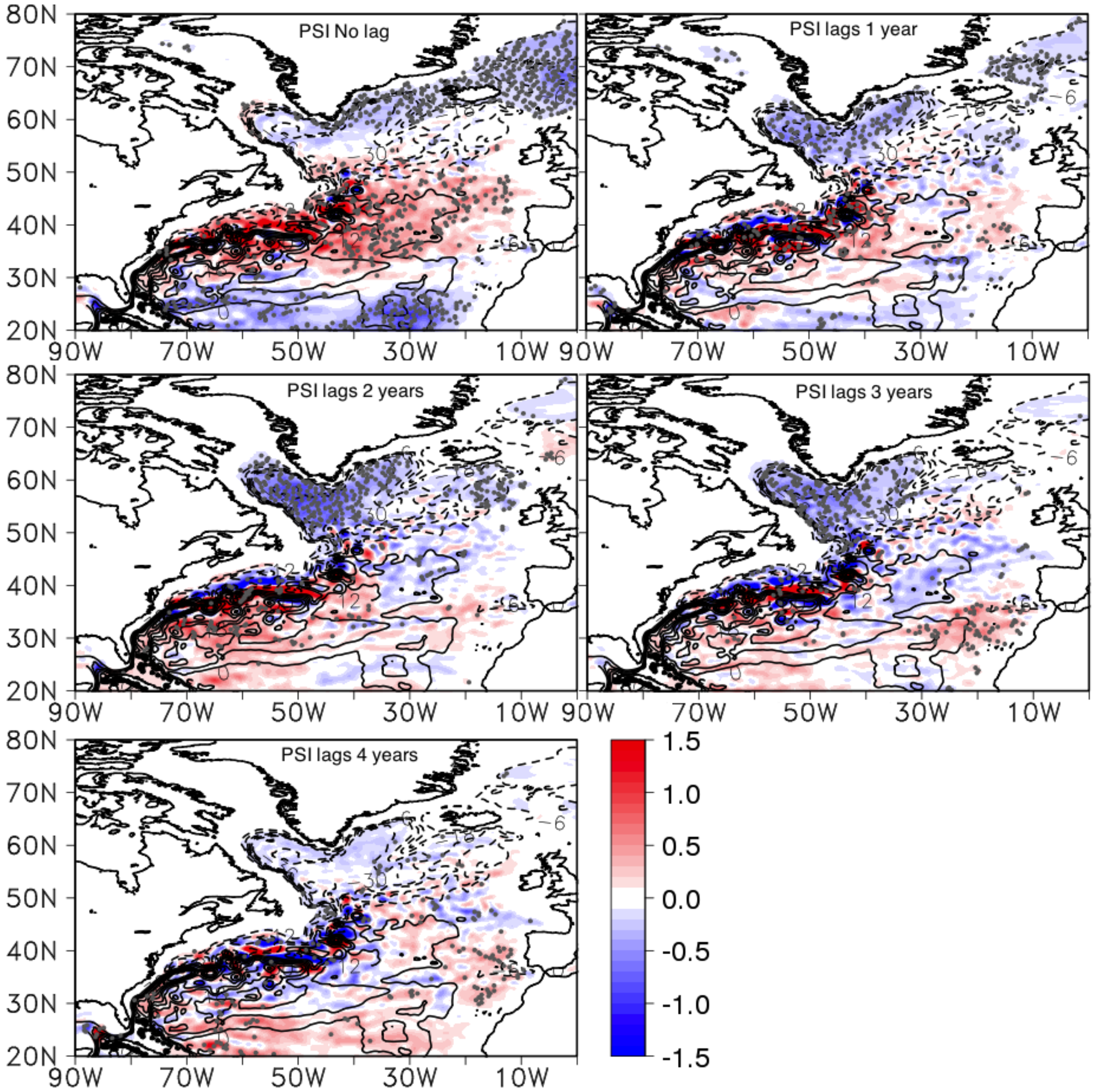

Figure 12 Linear regression coefficient of annual mean barotropic streamfunction onto the winter NAO index at time-lags 0-4 years (in Sv per unit change in NAO index) in shaded. The NAO index leads for positive time-lags. The mean state of the barotropic streamfunction from 1982-2013 is in contours. Areas that pass 95% significant values are shown in dots.